Pramana – J. Phys. (2019) 93:51
https://doi.org/10.1007/s12043-019-1813-4

Influence of material parameters on the performance of niobium-based superconducting radiofrequency cavities

ARUP RATAN JANA[1,2],*, ABHAY KUMAR[1], VINIT KUMAR[1,2] and SINDHUNIL BARMAN ROY[1,2]

[1]Department of Atomic Energy, Raja Ramanna Centre for Advanced Technology, Indore 452 013, India
[2]Department of Atomic Energy, Homi Bhabha National Institute, Mumbai 400 094, India
*Corresponding author. E-mail: arjana@rrcat.gov.in

MS received 21 September 2018; revised 14 February 2019; accepted 25 March 2019; published online 10 July 2019

Abstract. A detailed thermal analysis of a niobium (Nb)-based superconducting radiofrequency (SRF) cavity in a liquid helium bath is presented, by taking into account the temperature and magnetic field dependence of surface resistance and thermal conductivity in the superconducting state of the starting Nb material (for SRF cavity fabrication) with different impurity levels. The drop in SRF cavity quality factor (Q_0) in the high acceleration gradient regime (before the ultimate breakdown of the SRF cavity) is studied in detail. It is argued that the high-field Q_0-drop in SRF cavity is considerably influenced by the intrinsic material parameters such as electrical conductivity and thermal diffusivity. The detailed analysis reveals that the current specification on the purity of Nb material for SRF cavity fabrication is somewhat overspecified, as also inferred by the experimental work reported by some of the laboratories in the recent past. In line with these encouraging experimental results, in this paper, based on a rigorous calculation, we show that the Nb material with relatively low purity can very well serve the purpose for the accelerators dedicated for spallation neutron source (SNS) or accelerator-driven subcritical system (ADSS) applications, where the required accelerating gradient is typically up to 20 MV m^{-1}. This information will have important implication towards the cost reduction of superconducting technology-based particle accelerators for various applications. We think this theoretical work will be complementary to the experimental efforts performed in various laboratories at different corners of the globe.

Keywords. Cavity quality factor; electrical surface resistance; niobium; accelerators; superconducting radio frequency cavities; thermal conductivity.

PACS Nos 74.25.fc; 73.20.Hb; 72.15.Eb; 71.55.Ak; 29.20.Ej

1. Introduction

One of the remarkable developments in the area of particle accelerators in modern times has been the successful use of the state-of-the art superconducting radiofrequency (SRF) cavities in building high-energy linear accelerators (linacs) [1–5]. Compared to a normal conducting radiofrequency (RF) cavity, in an SRF cavity, the heat dissipation is significantly less. Therefore, the SRF cavities are quite attractive choices for high-energy–high-current accelerators, operating in the continuous wave or long pulse mode [5,6]. The low-loss feature of an SRF cavity is characterised by its extraordinary high value of quality factor Q_0 ($\sim 10^{10}$), which is inversely proportional to the power loss P_c at the cavity wall [1,5,7]. The superconducting material used for making the SRF cavity is characterised by its surface resistance R_s in the superconducting state at the operating frequency. The power loss of an SRF cavity is proportional to R_s, which implies that Q_0 will be inversely proportional to R_s [5,7].

Niobium (Nb) is the material of choice for making SRF cavities because of its relatively high value of superconducting transition temperature or critical temperature T_c ($\sim$9.2 K) as well as the lower critical magnetic field B_{c1}, relative abundance and ease in availability, and mechanical strength as well as formability. Experimentally, Q_0 of a Nb-SRF cavity shows the following typical trend with the increasing strength of the amplitude B_a of the RF magnetic field at the cavity surface: it first increases slightly in the very low field ($B_a \sim$0–20 mT), then it decreases gradually in the

medium field regime ($B_a \sim 20$–80 mT), and finally, a sharp fall occurs at higher RF fields ($B_a \sim 80$–180 mT), which is known as the Q_0 drop [8,9]. This sharp fall in Q_0 indicates the breakdown of superconductivity in the SRF cavity material. The corresponding value of B_a at which this happens is known as the threshold magnetic field B_{th} [10,11]. In recent times, there is a continual quest in the SRF community to push this threshold limit B_{th} towards B_{c1} (or beyond) of Nb to achieve a higher value of accelerating gradient E_{acc}, and simultaneously a higher value of Q_0 to make the higher energy accelerators economically more viable.

More importantly, the observed threshold value B_{th} of Nb-SRF cavities depends on the quality of the starting Nb material, as well as the processing techniques used during the cavity development. The high purity of the Nb material ensures a higher value of thermal conductivity κ in the normal state and the cavity processing removes the surface damage of the Nb material, which takes place in the course of forming an SRF cavity. However, at the typical operating temperature of 2 K in the superconducting state of Nb, the value of κ reduces significantly from its value in the normal state just above T_c [1,5]. Therefore, the heat removal turns out to be a crucial issue, even though the rate of heat generation may be small in the case of an SRF cavity.

In order to realise the goal of high accelerating gradient accompanied with high Q_0, the prevalent practice followed in the SRF community is to use highly pure Nb, mainly to achieve a higher normal state thermal conductivity [1]. The purity of a metal is often characterised by the residual resistivity ratio (RRR), which is usually defined as the ratio of the resistivity of the metal at room temperature and at a low enough temperature, where the resistance of the metal has reached its residual resistance limit [1,5,6]. Contemporary SRF community has set the value of RRR $= 300$, as the most recommended choice for the Nb material for SRF cavity fabrication. Experimental observations are there both in favour as well as against this empirical choice of standard for RRR [6]. To explain this breakdown phenomenon, as well as to predict the breakdown field, several interesting theoretical analyses have been reported in the past. Amongst these, in the analyses reported in refs [12,13], R_s is assumed to be independent of B_a, and is a function of temperature alone. In order to develop a more realistic model, one must consider the dependency of R_s on the applied field B_a. This field-dependent R_s is known as the nonlinear Bardeen–Cooper–Schrieffer (BCS) surface resistance. Weingarten [14] and Gurevich [15] have taken this nonlinearity into account, and have performed more rigorous analyses of the thermal breakdown phenomenon. Bauer *et al* [16] discussed a theoretical thermal feedback model (TFBM) including the nonlinear BCS resistance, which explains the experimental results for different SRF cavities. However, in refs [14–16], they have calculated the heat load after considering the local ohmic relation. In addition, the analysis presented in ref. [16] expresses the nonlinear BCS surface resistance in the form of a power series in $(B_a/B_c)^2$ and keeps only the first-order term. They have introduced a free parameter $C(l, \omega, T)$ (eq. (9) in ref. [16]) to scale this term to attain a proper match with the experimental data. There is some arbitrariness in the choice of this free parameter, in order to explain the experimental data. Thus, although there is a good agreement between the experimental and calculated data as described in ref. [16], this approach is not directly useful in our calculation. Vines *et al* [17] used a similar approach where they have included the influence of non-local response of the electromagnetic field while calculating the surface resistance and taken a fixed value of $C(l, \omega, T) = 2$ to perform magnetothermal analysis to study the trend for the medium field Q_0-slope, considering a few values of RRR. They have, however, not calculated the value of the threshold magnetic field, but interestingly, their analysis indicates the increasing trend of the threshold magnetic field with the reduced value of RRR, which supports our results that will be discussed in this paper. The non-local response of the electromagnetic field is an important consideration in the calculation of R_s. The model described in ref. [18] implemented this concept of non-locality in the calculation of R_s. However, the field dependency of R_s is not included in their calculation. In the model used in our calculation, R_s is obtained by considering the non-local response of the electromagnetic field. More importantly, we have used the nonlinear BCS surface resistance in our calculation that has dependency on the applied field B_a. Gurevich [19] recently presented a new model for the nonlinear superconducting surface resistance based on density of state (DOS) smearing, which is applicable to Ti- or N-treated Nb cavities. This model is unique in the sense that it can very well explain the prominent field-induced suppression of surface resistance in Ti- or N-treated Nb cavities. As we consider the case of SRF cavities made of medium- or high-purity Nb material without doping, this particular model [19] is not directly applicable for our work.

Most of the analyses of the thermal breakdown phenomena do not consider the temperature dependence of thermal conductivity κ of Nb in spite of the same being significant. A more complete approach will therefore be to include the dependence of temperature on κ, and dependencies of magnetic field as well as temperature on R_s in the analysis, for 'different purity levels of Nb'.

In this paper, we have followed this approach to perform a theoretical analysis of this magnetothermal process in a self-consistent manner.

Although the choice of RRR 300-grade Nb as the material for the superconducting cavity has been most popular in the SRF community, in the last two decades, extensive experimental work performed in several accelerator laboratories has shown a clear indication that the cavities made using lower RRR material are also able to meet the high gradient specifications. In this context, we mention the earlier attempts made in the late 1990s as described in ref. [20]. Several successful test results obtained in the XFEL project also strongly favour this idea [21]. Ciovati *et al* [22] nicely summarise the dependency of the quality factor on the electromagnetic field of the cavity and clearly show that the cavities (with resonating frequency between 1.3 and 2.3 GHz) made of RRR 100-grade Nb can be successfully operated with a peak surface magnetic field around 100 mT, after passing through appropriate pre-processing. As shown in ref. [23], an appropriate pre-processing is crucial to achieve the requirement of high gradient operation. In light of these encouraging results, we have performed an extensive magnetothermal analysis, which will be complementary to the experimental efforts performed in different laboratories. Our theoretical formulation has been benchmarked against observations of the performance of tera electron volt energy superconducting linear accelerator (TESLA) superconducting cavities, and we extend our approach to establish an optimal purity level of the Nb material of the SRF cavity for the proton accelerators dedicated for spallation neutron source (SNS) or accelerator-driven subcritical system (ADSS) applications.

The analysis presented in this paper is for 1.3 GHz, which is the operating frequency for the TESLA cavities [1] for the proposed linear electron–positron collider. Similar type of elliptic SRF cavities with fundamental frequency of 650 MHz will also be used in the injector linac for the proposed Indian spallation neutron source (ISNS) project [24,25] as well as other projects such as Chinese-ADS program [26] and PIP-II project [27].

The paper is organised as follows. Section 2 discusses the analytical models used to calculate the thermal conductivity κ and superconducting surface resistance R_s as a function of (i) the purity level of the Nb material, (ii) RF magnetic field amplitude B_a at the cavity surface and (iii) temperature T. Next, in §3, we present the results of our magnetothermal analysis, where we highlight the influence of the purity level of Nb on the electromagnetic response of an Nb-SRF cavity. Finally, in §4 we discuss the important inferences that can be drawn from the analysis presented in this paper, and conclude.

2. Theoretical formulation

2.1 *Generalities*

The quality factor Q_0 of an SRF cavity is evaluated using the formula $Q_0 = G/R_s$, where G is solely dependent on the geometry of the cavity, and is known as the geometry factor [5,7]. If we assume that R_s is field-independent, then Q_0 will have a very weak dependency on B_a, and should remain nearly constant up to the breakdown limit. But the experimentally observed quality factor is associated with a Q_0-slope [1,5]. Also, the breakdown does not occur at a sharp value of B_a. Instead, it occurs over a range of B_a. This implies that R_s should have some direct or indirect functional dependency on B_a [14,15]. This will be discussed in the next subsection.

It may be appropriate to present here a brief discussion on the purity level of the material. For Nb, mostly the defects are of two types: (i) impurities due to metallic (e.g. Ta, Fe, Sn, etc.) or non-metallic (e.g. O, H, etc.) inclusions and (ii) various kinds of material defects including dislocations [28]. Although the first type of defect is reduced by following an expensive processing and purification process of Nb material, the second type of defect, i.e. dislocations, is unavoidable even in very pure Nb. The amount of such defects will actually increase during the half-cell formation of an elliptical Nb-SRF cavity, and thus the RRR of the Nb material in a finished product of Nb-SRF cavity will be significantly different from the RRR of the starting Nb material. In general, the electronic mean free path (l_e) of a metal is a function of the purity level of that material [5, 14,22,29]. The normal state electrical resistivity (ρ_{no}) of a metal can be estimated from the value of the mean free path l_e. For Nb, at $T_c = 9.2$ K, we can write $l_e = (3.7 \times 10^{-16}\ \Omega\,m^2)/\rho_{no}$ [28]. We would like to emphasise that for the normal electrons, the value of ρ_{no} as well as l_e remain almost unaltered in Nb in the temperature range below T_c. As already mentioned, the commonly followed approach to quantify the purity level in Nb is in terms of RRR, which is the ratio between the resistivity $\rho_{300\,K}$ at 300 K and the normal state resistivity (ρ_{no}) at a sufficiently low temperature, say at 9.2 K, i.e. just above the superconducting transition temperature. Therefore, the RRR will be proportional to l_e, assuming that $\rho_{300\,K}$ is nearly independent of the purity level of the material. In the next subsections, we shall explain how the level of impurity plays an important role in deciding R_s and κ of a material.

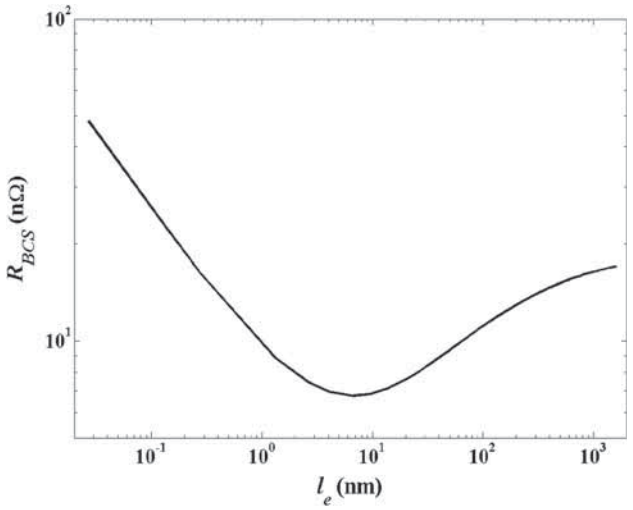

Figure 1. Plot of R_{BCS} (calculated using the non-local response of electric field) at 2 K as a function of l_{e} for Nb. Here, $\lambda_0 = 39$ nm, $\xi_0 = 32$ nm and $\Delta = 1.9k_{\mathrm{B}}T_{\mathrm{c}}$.

2.2 *Electrical surface resistance (R_{s})*

The surface resistance R_{s} of a superconducting material is the sum of BCS resistance R_{BCS} and the residual resistance R_i. R_{BCS} has a strong dependence on the electronic mean free path l_{e}. In the dirty limit, l_{e} is much less than the zero field coherence length ξ_0, and is therefore adequately small. RF field in this case remains nearly constant during the time interval between two collisions. This scenario changes with the increasing level of purity of the material, and in the clean limit ($l_{\mathrm{e}} \gg \xi_0$), the temporal variation of the field is noticeable during the time interval between two collisions. Current density is no more merely a function of the local electric field in that case. In order to include this non-local response of electromagnetic fields, we followed a procedure adopted in the computer code SRIMP [30,31], which uses the full BCS theory in the calculation of R_{BCS}. Figure 1 shows the plot of R_{BCS} at a constant temperature 2 K, as a function of l_{e} near 'zero magnetic field', i.e. $B_{\mathrm{a}} \to 0$ mT. As shown in the figure, after a shallow minimum near $l_{\mathrm{e}} \sim 10$ nm, the value of R_{BCS} increases gradually with l_{e} in the clean limit of the superconducting material. We would like to mention here that in the dirty limit, the calculated values of R_{s}, considering the non-local field responses are very close to the value obtained using the local field responses, as expected. However, in the clean limit, there is a significant variation in the value of R_{s} calculated using these two approaches. As an example case of Nb with $l_{\mathrm{e}} = 270$ nm, R_{s} is nearly two times less if we perform the calculation after considering the non-local field response.

In order to calculate R_{BCS} using this formulation, we considered the 'zero-temperature' coherence length ξ_0 and London penetration depth λ_0 as 39 and 32 nm, respectively [32], and the superconducting band gap $\Delta = 1.9k_{\mathrm{B}}T_{\mathrm{c}}$, where k_{B} is the Boltzmann constant.

In the presence of an applied magnetic field B_{a}, the expression of R_{s} gets modified. Following the work of Gurevich [15], for a type-II superconductor in the clean limit, the modified $R_{\mathrm{s}}(T, l_{\mathrm{e}}, B_{\mathrm{a}})$ can be written as follows:

$$R_{\mathrm{s}} = \frac{8R_{\mathrm{BCS}}(l_{\mathrm{e}})}{\pi {\beta_0}^2} \int_0^{\pi} \sinh^2\left(\frac{\beta_0}{2}\cos\tau\right) \tan^2\tau \, \mathrm{d}\tau + R_i, \tag{1}$$

where

$$\beta_0 = \frac{\pi}{2^{3/2}} \frac{B_{\mathrm{a}}}{B_{\mathrm{c}}} \frac{\Delta(T)}{k_{\mathrm{B}}T},$$

B_{c} is the thermodynamic critical magnetic field, which is 200 mT for Nb [15]. Note that the residual resistance R_i, which is present even at zero temperature, has its origin in trapped magnetic flux, formation of niobium hydride islands near the surface, etc. [22]. Based on the experimentally observed values, we have assumed a value of 5 nΩ for R_i in our analysis. Hence, considering $R_i = 5$ nΩ, we perform a precise calculation for the surface resistance as a function of temperature, purity level of the superconducting Nb material and magnetic field, using eq. (1).

In the next subsection, we shall discuss the dependence of thermal conductivity of Nb on different parameters, in the superconducting state.

2.3 *Thermal conductivity of the SRF cavity material*

There are two types of heat carriers in a metal – the conduction electrons and the lattice vibrational modes, i.e. phonons [5,29,33,34]. Amongst these two, in typical metals, the electronic contribution dominates. The total thermal conductivity $\kappa(T)$ of a metal is the summation of these two contributions, i.e. $\kappa(T) = \kappa_{\mathrm{en}}(T) + \kappa_{\mathrm{L}}(T)$ [33,34]. The electronic contribution to the thermal resistivity arises because of the scattering of normal electrons from lattice imperfections due to the thermal vibrations as well as various defects (including impurities) present in the material [34]. The latter can be estimated using the Wiedemann–Franz law (at low temperatures), which is stated as $\kappa_{\mathrm{ei}}(T) = L_0\sigma_{\mathrm{no}}T$ [29], where L_0 is the Lorentz number. Considering the contribution from the electron–lattice scattering, i.e. $\kappa_{\mathrm{el}} = 1/aT^2$, where a is constant, the total electronic thermal conductivity can be written as $\kappa_{\mathrm{en}}(T) = (1/L_0\sigma_{\mathrm{no}}T + aT^2)^{-1}$. As discussed in the previous paragraph, with the increase in the purity level of the material, its electrical conductivity σ_{no} increases

and so does $\kappa_{en}(T)$. Hence, the material in its purest form will offer the best thermal conductivity.

In the superconducting state of a metal, the number of free electrons reduces because of the formation of Cooper pairs. This results in a scaled-down contribution in the electronic thermal conductivity $\kappa_{es}(T)$ of a superconductor. This scale factor $R(y)$, as given by Bardeen *et al* [35], is as follows:

$$\frac{\kappa_{es}}{\kappa_{en}} = R(y) = \frac{1}{f(0)}\left[f(-y) + y\ln(1+e^{-y}) + \frac{y^2}{2(1+e^{-y})}\right], \quad (2)$$

where $f(-y)$ is the Fermi integral, which is defined as $f(-y) = \int_0^\infty (z/[1+\exp(z+y)])dz$ and $y = \Delta(T)/(2\kappa_B T)$. As shown in ref. [35], the value of $R(y)$ tends to 0 as T tends to 0, and approaches unity as we approach the transition temperature (i.e. $T \to 9.2$ K).

In our analysis, we have estimated κ_{en} for different values of impurity levels, i.e. for different values of $\sigma_{no}(l_e)$, and to calculate the normal state thermal conductivity of Nb at 9.2 K, we have used $L_0 = 2.45 \times 10^{-8}$ W K^{-2} [29,33] and $a = 7.52 \times 10^{-7}$ mW^{-1} K^{-1} [34], respectively.

Unlike the free electrons, crystal lattice contributes in a relatively small amount in the total thermal conductivity. The total $\kappa(T)$ for a material in its superconducting state can be estimated from the following equation [33,34]:

$$\kappa(T) = \kappa_{es}(T) + \kappa_L(T) = \frac{R(y)}{\left((1/L\sigma_{no}T) + aT^2\right)} + \left(\frac{1}{DT^2e^y} + \frac{1}{Bl_{ph}T^3}\right)^{-1}. \quad (3)$$

Here, the second part on the right-hand side of the equation is the phononic contribution due to the lattice, where D and Bl_{ph} are the two constants, and l_{ph} is the phonon mean free path. The values of these two constants depend on different levels and types of post-processing [5,36] that the cavity has undergone. For a defect-free metal with high purity, there is the likelihood of a phonon peak at a very low temperature (around $T = 2$ K), which can result in an enhancement in $\kappa_L(T)$. However, for a non-annealed SRF cavity, defects and dislocation introduced during the process of forming an SRF cavity destroys the phonon peak, partly or sometimes completely. These conditions, however, improve with the post-processing of an SRF cavity. Figure 2 shows the variation of thermal conductivity of Nb with temperature for three different cases, calculated using eq. (3). First, the case of pre-strained, small grain sample of Nb is considered, which shows a phonon peak in thermal conductivity near 2 K [36].

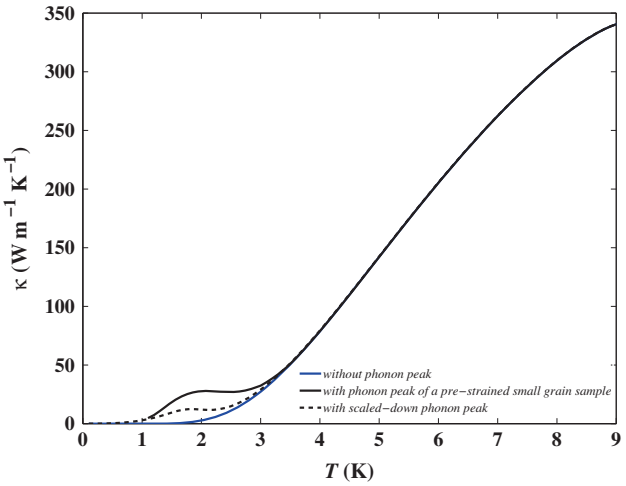

Figure 2. Total thermal conductivity κ of RRR 300-grade Nb as a function of temperature T. The blue curve denotes the case without the phononic contribution. Enhancement in κ at low temperature due to phonons is observed in a pre-strained, small grain Nb sample [36], as shown in the continuous black curve. The dotted black curve shows the case with reduced phonon peak in $\kappa(T)$, in accordance with experimental observation in ref. [16] for an SRF cavity.

Here, $D = 350$ mK^3 W^{-1} and $Bl_{ph} = 0.25$ mK^4 W^{-1} have been considered in the calculation. The second case is without the phononic contribution. Finally, the third case corresponds to a practical situation, where the phonon peak is not completely destroyed, but is scaled down suitably in accordance with the experimentally observed results at 2 K in ref. [16].

As expected, improvement in $\kappa_L(T)$ is more effective if we keep the liquid helium bath temperature $T_B = 2$ K. The phonon peak has almost no effect if we consider the bath temperature to be equal to 4.2 K.

The thermal conductivity of Nb is dependent on the applied RF magnetic field. However, we did not incorporate this dependency in our calculation. This is because in a superconducting cavity, the RF electric and magnetic fields almost vanish in the bulk of the material.

Next, we discuss the Kapitza resistance that is developed at Nb–He bath interface, and contributes prominently in the low-temperature regime, causing a temperature jump $\Delta T = (T_S - T_B)$ across the interface, where T_S is the temperature of the outer wall of the cavity. The value of ΔT determines the amount of heat flow $\bar{Q}$ per unit interface area per unit time, given by $\bar{Q} = h_k(T_S - T_B)$. Here, h_k is the Kapitza conductance, which is a function of T_S and T_B. It is estimated in units of W m^{-2} K^{-1} from the following equation for $T_B \sim 2$ K [37]:

$$h_{\mathrm{k}} = 200 T_{\mathrm{S}}^{4.65} \left[1 + \frac{3}{2} \left(\frac{T_{\mathrm{S}} - T_{\mathrm{B}}}{T_{\mathrm{B}}} \right) + \left(\frac{T_{\mathrm{S}} - T_{\mathrm{B}}}{T_{\mathrm{B}}} \right)^2 + \frac{1}{4} \left(\frac{T_{\mathrm{S}} - T_{\mathrm{B}}}{T_{\mathrm{B}}} \right)^3 \right]. \quad (4)$$

Hence, finally in the steady-state condition, the heat balance equation is written as

$$\frac{1}{2\mu_0^2} R_{\mathrm{s}}(T_{\mathrm{s0}}, B_{\mathrm{a}}, l_{\mathrm{e}}) B_{\mathrm{a}}^2 = -\kappa(T, l_{\mathrm{e}}) \nabla(T) = h_{\mathrm{k}}(T_{\mathrm{S}} - T_{\mathrm{B}}). \quad (5)$$

Here, T_{s0} is the steady-sate temperature of the inner wall of the cavity.

3. Numerical calculations and analysis of the results

In this section, we discuss the results of our magnetothermal analysis, where the purity level of the material is considered as an input parameter. In this analysis, the inner surface of the SRF cavity is the source of the outward heat flux, which is then diffused through the thickness of the wall, and is finally dissipated in the liquid helium bath maintained at the constant temperature T_{B}. The amount of heat flux depends on $R_{\mathrm{s}}(T, B_{\mathrm{a}}, l_{\mathrm{e}})$, and the rate of heat diffusion is controlled by $\kappa(T, l_{\mathrm{e}})$ as well as $h_{\mathrm{k}}(T_{\mathrm{s}}, T_{\mathrm{B}})$. R_{s}, κ and h_{k} are calculated using the formulation described in the previous section. We then use eqs (4) and (5) to find out the temperature of the inner surface of the cavity in the steady state. The surface resistance R_{s} is evaluated at this temperature, including the effect of B_{a}, for the given value of l_{e}. The quality factor Q_0 is then calculated using this value of R_{s}.

In the remaining part of this section, we perform the calculations of a 1.3 GHz SRF cavity, taking the functional dependency of R_{s}, κ and h_{k} into account. We first described the details of problem modelling, followed by the presentation of results of numerical calculations.

3.1 *Simulation model*

Figure 3 describes the model, which is a 2.8-mm thick, infinite Nb slab with planar geometry. One side of this slab is exposed to a spatially uniform RF field resonating at 1.3 GHz, whereas the other side is in contact with liquid helium at a bath temperature T_{B}. From the symmetry of the problem, the heat diffusion equation will be one-dimensional (1D) here.

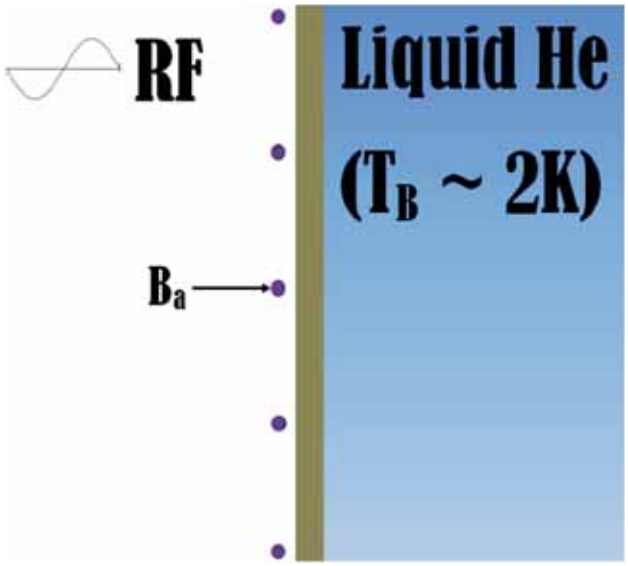

Figure 3. Geometry of a 2.8-mm thick infinite Nb plate used as the model. Here, the 'dots' represent the applied magnetic field B_{a} on the surface. The inner surface of the plate is in vacuum and the outer surface is immersed in a liquid helium bath at 2 K.

3.2 *Numerical calculations and results*

In order to obtain steady-state solutions for the converged values R_{s} and κ, computer programs were written in MATLAB. Detailed magnetothermal calculations were performed for all the three scenarios, as shown in figure 2. We first performed the magnetothermal analysis after considering a fixed value of $\sigma_{\mathrm{no}} = 2.069 \times 10^9$ $(\Omega\ \mathrm{m})^{-1}$. Using the expression for RRR given in refs [1,5], this corresponds to RRR $\sim$ 300. Figure 4 shows the variation of Q_0 as a function of the applied magnetic field B_{a} for the geometry shown in figure 3.

As shown in figure 4, the approximate value of B_{th} at which there is a sharp change in the rate of decrease in Q_0 is 114 mT when we do not consider the phononic contribution in $\kappa(T)$. The value of B_{th} increases to 154 mT when we consider full phononic contribution in $\kappa(T)$, and to 130 mT when we consider a scaled-down phononic contribution. It is important to note that in the vicinity of B_{th}, the temperature is well beyond where the phonon peak occurs. Even then, the presence of phonon peak affects the value of B_{th}. This is because of the high sensitivity of cavity surface temperature with magnetic field near the breakdown. Using the ratio of peak surface field B_{pk} to accelerating field E_{acc} specified for the optimised geometry of TESLA cavity in ref. [1], we obtained the maximum achievable value of acceleration gradient E_{acc} as 27, 30 and 36 MV m^{-1} for the cases of no phononic contribution,

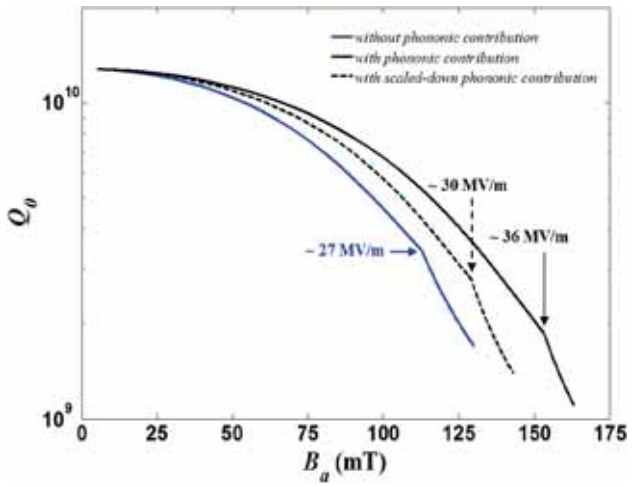

Figure 4. Plot of Q_0, as a function of B_a for 1.3 GHz TESLA cavity made of RRR 300-grade Nb, considering three possible variations of $\kappa(T)$ described in figure 2.

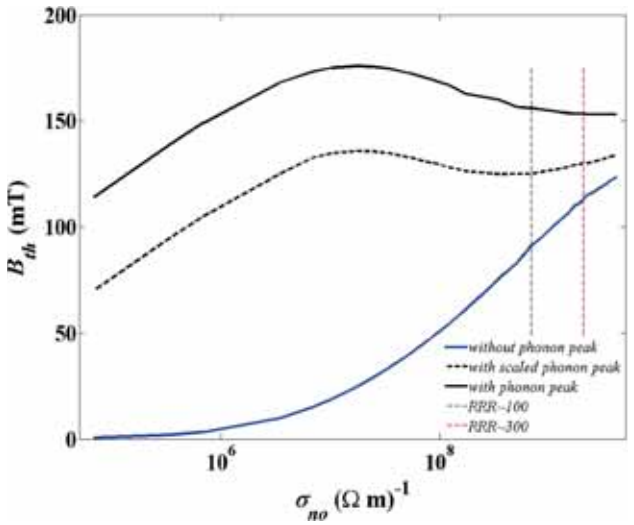

Figure 5. Plot of B_{th} as a function of σ_{no} for 1.3 GHz TESLA cavity. Here, the blue curve corresponds to the case where the phononic contribution is not considered, whereas the continuous and dotted black curves correspond to the case of full phononic contribution and scaled-down phononic contribution, respectively.

scaled-down phononic contribution and full phononic contribution, respectively. We would like to point out that our theoretical prediction without the phonon peak is in good agreement with the experimentally reported observation in figure 12 of ref. [1], where a similar trend is seen and a similar value is obtained for maximum achievable E_{acc}. Our result after considering the contribution of full phononic contribution agree with the experimentally obtained value of ∼40 MV m^{-1} in ref. [16]. A reasonable agreement between the experimentally obtained results and the results of our analytical calculation benchmarks the approach followed in our analysis.

Next, we repeat the calculation for different values of σ_{no} and obtain the threshold values of the RF magnetic field B_{th} as a function of σ_{no}, for the case without phonic contribution, as shown in figure 5. In this case, B_{th} initially shows a rapid and monotonic rate of rise with σ_{no}. However, this rate decreases for higher values of σ_{no} corresponding to high purity of Nb.

Next, we discuss the case with full phononic contribution. Here, interestingly, B_{th} initially increases with σ_{no}, reaches a maximum value of ∼176 mT at $\sigma_{no} \sim 1.724 \times 10^7 (\Omega\ m)^{-1}$, and finally for higher value of σ_{no}, B_{th} saturates at ∼153 mT. For the case with scaled-down phononic contribution, B_{th} reaches the maximum value of 134 mT at $\sigma_{no} \sim 1.724 \times 10^7 (\Omega\ m)^{-1}$, and saturates at ∼125 mT for higher values of σ_{no}. Based on these results, we can make interesting comparison between the expected performances from RRR 300- and RRR 100-grade Nb cavities. For the case with phononic contribution, B_{th} is nearly the same for RRR 300 and RRR 100 cases. On the other hand, for the case without phononic contribution, B_{th} decreases from 114 mT for the RRR 300 case to 91 mT for RRR 100 case. We would like to emphasise here that based on the beam dynamics considerations, the requirement on maximum acceleration gradient in 1 GeV proton accelerators for SNS or ADSS applications is modest, and typically less than 20 MV m^{-1}. A stable beam with low beam loss is the primary criterion there. Based on our detailed magnetothermal analysis, it appears that the relatively impure Nb with RRR 100-grade Nb will give performance similar to RRR 300-grade material, and may therefore be acceptable. For the proposed ISNS project at RRCAT, Indore, we have performed the calculations of Q_0 and B_{th} for the 650 MHz elliptical SRF cavity geometry described in ref. [25]. These calculations are presented in figure 6, where the variation of Q_0 as a function of the applied magnetic field B_a is shown for a fixed value of $\sigma_{no} = 6.89 \times 10^8 (\Omega\ m)^{-1}$ corresponding to RRR 100-grade Nb.

For high average power accelerator for SNS or ADSS applications, the cryogenic heat load is an important consideration. Hence, for such cases, it will be more practical to restrict the operating gradient of the cavity up to a value, where the Q value drops down to not more than 50% of the zero field Q value. With these considerations, as seen from figure 6, the maximum magnetic field of ∼109 mT can be supported at the cavity surface for the case, where we do not consider the phononic contribution. This value changes to ∼140 mT when we consider the full phononic contribution, and to ∼129 mT when we consider a scaled-down phononic

contribution. For these cavities, the design value of $B_{\rm pk}/E_{\rm acc}$ is 4.56 mT (MV m)$^{-1}$ [25], which implies that even without considering any phononic contribution, we can go for an $E_{\rm acc}$ of $\sim$24 MV m^{-1} with RRR 100-grade Nb, which is sufficient to fulfil the requirement. Another added advantage of using relatively impure RRR 300-grade Nb will be that it will give nearly 10% higher value of quality factor in comparison with the cavities made of high-purity RRR 300-grade Nb. For an easy reference, values of the cavity quality factor (Q) at their threshold values of the magnetic field ($B_{\rm th}$) are tabulated for the 1.3 GHz TESLA cavity, as well as for the 650 MHz ISNS cavity (see tables 1 and 2).

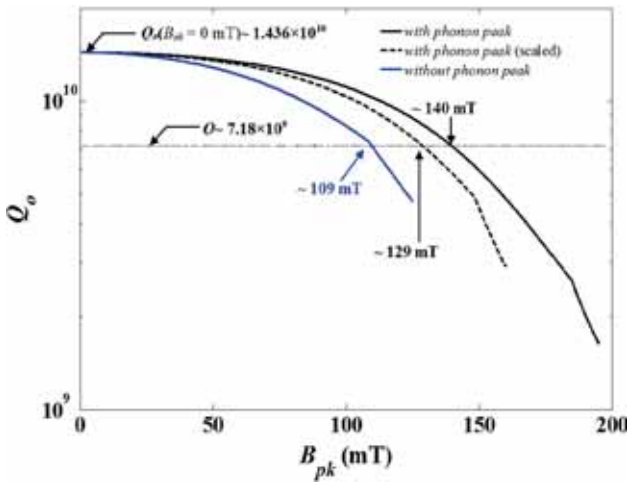

Figure 6. Plot of Q_0 as a function of $B_{\rm a}$, as obtained from the analysis performed on an ISNS cavity [25] for a fixed value of RRR 100-grade Nb, for three possible variations of $\kappa(T)$. For these calculations, we considered 4-mm thick plate geometry. We have taken $R_i = 10$ nΩ in this analysis.

4. Discussions and conclusions

In this paper, we have revisited the correlation between the purity level of the Nb-SRF material, and the threshold magnetic field value $B_{\rm th}$ for the magnetothermal breakdown of an SRF cavity. In our analysis:

(1) $\sigma_{\rm no}$ was used as a measure of the purity level of the Nb material;
(2) $R_{\rm s}$ and κ were calculated as a function of T, $B_{\rm a}$ and the purity level of the material;
(3) Kapitza resistance was estimated as a function of $T_{\rm B}$ and $T_{\rm S}$.

As a first step of our analysis, we presented a case study for the 1.3 GHz TESLA cavity, considering a constant value of $\sigma_{\rm no} \sim 2.069 \times 10^9$ $(\Omega\,{\rm m})^{-1}$, which corresponds to RRR 300-grade Nb. Considering the bath temperature $T_{\rm B} = 2$ K, we evaluated the maximum achievable acceleration gradient in the cavity, limited by the magnetothermal breakdown of superconductivity. Agreement of our results with the experimentally reported observations in ref. [1] validates our approach. After benchmarking our magnetothermal analyses, we used this approach to study the influence of material purity on the performance of Nb-based SRF cavity. Calculations performed without considering the phononic contribution in thermal conductivity show that for medium RRR grade Nb, $B_{\rm th}$ marginally increases with material purity. Interestingly, when we consider the phononic contribution that gives rise to phonon peak in thermal conductivity, $B_{\rm th}$ reaches a maximum for modest values of RRR, after which it decreases and nearly saturates. We compared $B_{\rm th}$ for an SRF cavity made of RRR 100-grade Nb with that made using RRR 300-grade Nb. Based on our

Table 1. Q-values at $B_{\rm th}$ for 1.3 GHz TESLA cavity.

	RRR 300-grade Nb		RRR 100-grade Nb	
	$B_{\rm th}$ (mT)	$Q(B_{\rm th})$	$B_{\rm th}$ (mT)	$Q(B_{\rm th})$
Without phonon peak	115	3.28×10^9	92	4.94×10^9
With scaled phonon peak	131	2.67×10^9	126	3.35×10^9
With phonon peak	154	1.84×10^9	157	2.04×10^9

Table 2. Q-values at $B_{\rm th}$ for 650 MHz ISNS cavity.

	RRR 300-grade Nb		RRR 100-grade Nb	
	$B_{\rm th}$ (mT)	$Q(B_{\rm th})$	$B_{\rm th}$ (mT)	$Q(B_{\rm th})$
Without phonon peak	134	5.20×10^9	109	7.27×10^9
With scaled phonon peak	154	3.92×10^9	147	5.00×10^9
With phonon peak	180	2.46×10^9	184	2.64×10^9

magnetothermal analysis, we find that B_{th} is marginally lower for RRR 100-grade Nb than for RRR 300-grade Nb, but still acceptable for building 1 GeV proton H^- linac for SNS or ADSS applications, and provides nearly 10% higher value of quality factor. We would like to mention that in our calculation, we have taken the residual resistance as 5 and 10 nΩ for 1.3 GHz TESLA cavity and 650 MHz ISNS SRF cavity, respectively, which are the typical values. With improvement in various processes, the trapped magnetic flux and other components of the residual resistance can be further reduced which will lead to the enhancement in the Q_0 value compared to that reported in this paper.

We would like to mention that the results presented in this paper were obtained, after considering the plate geometry of the cavity material, in order to keep the analysis simple and one-dimensional. We clarify that we have also repeated the calculation with a three-dimensional (3D) model of an elliptic SRF cavity half-cell in ANSYS using ANSYS®APDL, where, considering the azimuthal symmetry of the cavity geometry, only a 15° sector of the half-cell was modelled to minimise the computational effort. The field profile used in that calculation was obtained from the electromagnetic eigenmode analysis of the cavity. The results obtained using this model were within 10% of the results obtained using the simplified plate geometry. The proximity between these two sets of results establishes that the heat flows effectively in one direction as the cavity wall thickness is much smaller than the surface curvature, as also observed in ref. [17].

Our study shows that although RRR 300-grade Nb might help in increasing the threshold acceleration gradient for high gradient applications such as International Linear Collider [38], RRR 100-grade should be acceptable for making 1 GeV superconducting linac for SNS/ADS applications. Thus, for such applications, the required value of RRR can be reduced to 100 from 300, which is currently followed as the desired specification by the SRF community worldwide. From our literature study, we could not find a strong basis behind the choice of RRR 300-grade Nb for such applications that require acceleration gradient up to 20 MV m^{-1}. As mentioned in ref. [39], the choice was based on the availability of pure Nb materials with a gross assumption of superior superconducting properties in such high-purity materials. We thus believe that the choice of RRR 300-grade Nb is somewhat empirical, which might have been chosen under certain conditions, and then the trend was continued. There are some experimental results on SRF cavities that are made of Nb having RRR < 300 [17,18,20,21,40,41] which convey a similar point as discussed in §1. There, the observation of the increasing trend of the threshold magnetic field with the reduced value of RRR indeed supports our analysis.

Considering from the point of the view of the ease of availability, relatively impure Nb (of RRR 100-grade) can be the potential material for the fabrication of SRF cavities particularly for the purpose of SNS and ADSS applications. Table 4 of ASTM B393 shows that the mechanical strength of the RRR 100-grade (reactor grade) Nb is 30% higher than that of RRR 300-grade Nb. This gives further possibility of reducing the cavity thickness, which will benefit in two ways: (i) reducing the peak temperature at the cavity surface, thereby increasing the threshold field and (ii) bringing down the material weight for each cavity. Reactor-grade Nb has another interesting advantage compared to RRR 300-grade Nb, which is worth mentioning here. It is well known that during the cavity processing, hydrogen tends to go to the interstitial sites of Nb, leading to the formation of Nb hydride, which contributes significantly to the Q_0 drop during the cavity operation. In the case of reactor-grade Nb, hydrogen will more likely be trapped by impurity atoms or dislocations, which will reduce the chances of formation of niobium hydride at the interstitial sites.

We would like to emphasise that RRR alone does not decide the thermal conductivity of Nb. For example, even for fixed RRR, restoration of phonon peak by post-processing improves the thermal conductivity at around 2 K. For a given RRR, at low temperature, one can estimate the normal state electrical conductivity σ_{n_0}, and then the Wiedmann–Franz law can be used to estimate the thermal conductivity from σ_{no}. The Wiedmann–Franz law, however, estimates only one component κ_{ei} of the thermal conductivity arising due to electron impurity scattering, and one needs to add other contributions that cannot be directly estimated from RRR, as described in §2.3. Therefore, instead of specifying only RRR for the starting Nb material, we suggest that $\kappa(T)$ could also be an important parameter for Nb material specification. In order to understand the transient thermal response, one also needs to specify the diffusivity α of the material. Here, $\alpha = \kappa/(\rho \times C_P(T))$, where ρ and C_P [29] are the density and specific heat of the material. We thus believe that instead of specifying the RRR, we should specify σ_{no}, κ and α of Nb to get complete details of the material properties that determine the SRF cavity performance. Taking relatively impure Nb (of RRR 100-grade) as a material for cavity fabrication, we can specify these material parameters at 9.3 K as $\sigma_{\text{no}} \sim 6.89 \times 10^8\ (\Omega\ \text{m})^{-1}$, $\kappa \sim 138.68\ \text{W m}^{-1}\ \text{K}^{-1}$ and $\alpha \sim 0.005\ \text{m}^2\ \text{s}^{-1}$. Here, $C_P(T \sim 9.3\ \text{K}) = 3.36\ \text{J kg}^{-1}\ \text{K}^{-1}$ [42].

To further emphasise our point of view, here, we would like to mention the recent activities of nitrogen or titanium doping in Nb-SRF cavities [19,43,44], which result in lowering the mean free path, thus reducing the material purity/RRR at the surface, while maintaining a high value of material purity/RRR in the bulk. This helps in achieving lower value of surface resistance R_s, while maintaining a high value of bulk thermal conductivity κ. These recent trends corroborate our finding that lower RRR is helpful in getting better performance from Nb-SRF cavities. However, more importantly, in the case of 'Nb/Ti doping', one has to first produce high RRR Nb, which is expensive, and then dope at high temperature (typically 1000°C) with N_2 or Ti, which results in the threshold magnetic field of 90–100 mT [19] to obtain high Q_0. On the other hand, as suggested in our paper, it is economically more viable to use RRR 100-grade Nb, without any doping, with much higher threshold magnetic field.

In our analysis, we have considered the global breakdown phenomenon of the superconducting property of the Nb material in the context of an SRF cavity. In some cases, the local effect such as crack or microcrack on the surface, inclusion of a large bead of normal or magnetic material and/or rough welding pits/bumps may also cause hot spots, which in turn can trigger the breakdown of superconductivity of the material. Such extraneous effects can, however, be minimised by proper inspection and screening of the starting Nb materials, and implementing careful SRF cavity fabrication and post-processing techniques. The analysis presented in this paper can be extended to include the effect due to hot spots by adding an appropriate term in the expression of surface resistance, which will be taken up in future.

To conclude, we have analysed the effect of material purity on the threshold RF magnetic field value B_{th} at the cavity surface that determines the limiting acceleration gradient in an Nb-based SRF cavity. In this analysis, we have explicitly shown that it is possible to use relatively impure Nb (RRR 100) instead of expensive highly pure 300-grade Nb for building SRF cavities, especially for the SNS and ADSS applications. We believe that this is an advancement over the contemporary views where the role of material parameters is not adequately emphasised and choice of highly pure RRR 300-grade Nb is generally made. Based on our analysis, we argue that RRR 300-grade Nb may be an overspecification for the SNS and ADSS applications. This specification of Nb materials can be relaxed, which will have important implication in terms of a significant reduction in the cost of an Nb SRF cavity.

Acknowledgements

One of us (ARJ) would like to thank Amit Kumar Das for fruitful discussions. This work was supported by the Department of Atomic Energy, Government of India.

References

[1] B Aune *et al*, *Phys. Rev. ST Accel. Beams* **3**, 092001 (2000), https://doi.org/10.1103/PhysRevSTAB.3.092001

[2] R L Kustom, *Proceedings of the* 20th *International Linear Accelerator Conference* (Monterey, California, 2000) pp. 321–325, arXiv:physics/0008212

[3] S Henderson *et al*, *Nucl. Instrum. Meth. Phys. Res. A* **763**, 610 (2014), https://doi.org/10.1016/j.nima.2014.03.067

[4] D Boussard and T Linnecar, LHC project report 316, Presented at CEC-ICMC'99 (Montreal, Canada, 12–16 July 1999)

[5] H Padamsee, J Knobloch and T Hays, *RF superconductivity for accelerators* (Wiley, New York, NY, USA, 1998)

[6] S B Roy and G R Myneni, *AIP Conf. Proc.* **1687(1)**, 020006-1, https://doi.org/10.1063/1.4935320

[7] T P Wangler, Principles of RF linear accelerators, in: *Wiley series in beam physics and accelerator technology* (Wiley, New York, NY, USA, 1998) ISBN 0-471-16814-9

[8] G Ciovati *et al*, *Phys. Rev. ST Accel. Beams* **13**, 022002 (2010), https://doi.org/10.1103/PhysRevSTAB.13.022002

[9] G Cioviati, *Physica C* **441**, 44 (2006), https://doi.org/10.1016/j.physc.2006.03.126

[10] M Tinkham, *Introduction to superconductivity*, 2nd edn (Dover Publication, New York, NY, USA, 2004)

[11] W Weingarten, *Handbook of applied superconductivity* edited by B Seeber (IOP Publishing Ltd, 1998) Vol. 2, p. 1381

[12] H Safa, *Proceedings of the Workshop on RF Superconductivity* (Gif-sur-Yvette, France, 1995) pp. 413–418, http://epaper.kek.jp/SRF95/papers/srf95c10.pdf

[13] S H Kim and E I Campisi, *Phys. Rev. ST Accel. Beams* **10**, 032001 (2007), https://doi.org/10.1103/PhysRevSTAB.10.032001

[14] W Weingarten, *Phys. Rev. ST Accel. Beams* **14**, 101002 (2011), https://doi.org/10.1103/PhysRevSTAB.14.101002

[15] A Gurevich, *Physica C* **441**, 38 (2006), https://doi.org/10.1016/j.physc.2006.03.024

[16] P Bauer *et al*, *Physica C* **441**, 51 (2006), https://doi.org/10.1016/j.physc.2006.03.056

[17] J Vines, Y Xie and H Padamsee, *Proceedings of SRF* 2007 (Peking Univ., Beijing, China, 2007) pp. 178–191, https://www.classe.cornell.edu/rsrc/Home/Research/SRF/2007/TUP27.pdf

[18] D Reschke, *Proceedings of Workshop on RF Superconductivity* (Padova, Italy, 1997) pp. 385–396, https://accelconf.web.cern.ch/accelconf/SRF97/papers/srf97b13.pdf
[19] A Gurevich, *Phys. Rev. Lett.* **113**, 087001 (2014), https://doi.org/10.1103/PhysRevLett.113.087001
[20] D Barni, *Proceedings of* 10th *Workshop on RF Superconductivity* (Tsukuba, Japan, 2001) pp. 337–346, https://accelconf.web.cern.ch/accelconf/srf01/papers/ta009.pdf
[21] D Reschke *et al*, *Phys. Rev. ST Accel. Beams* **20**, 042004 (2017), https://doi.org/10.1103/PhysRevAccelBeams.20.042004
[22] G Ciovati, P Dhakal, P Kneisel and G R Myneni, *AIP Conf. Proc.* **1687**, 030001-1 (2015), https://doi.org/10.1063/1.4935322
[23] E Kako *et al*, *Proceedings of Workshop on RF Superconductivity* (Santa Fe, New Mexico, USA, 1999) pp. 180–186, http://epaper.kek.jp/SRF99/papers/tup011.pdf
[24] A R Jana, V Kumar, A Kumar and R Gaur, *IEEE Trans. Appl. Supercond.* **23(4)**, 3500816 (2013), https://doi.org/10.1109/TASC.2013.2256356
[25] A R Jana and V Kumar, *IEEE Trans. Appl. Supercond.* **24(6)**, 1 (2014), https://doi.org/10.1109/TASC.2014.2332435
[26] L Zhihui *et al*, *Phys. Rev. ST Accel. Beams* **16**, 080101 (2013), https://doi.org/10.1103/PhysRevSTAB.16.080101
[27] M Ball *et al*, *The PIP-II conceptual design report* edited by Valeri Lebedev (FANL, Batavia, USA, 2017) V0.00
[28] B B Goodman and G Kuhn, *J. Phys. Paris* **29**, 240 (1968), https://doi.org/10.1051/jphys:01968002902-3024000
[29] N W Ashcroft and N D Mermin, *Solid state physics*, 9th Indian Reprint (Cengage Learning, New Delhi, India, 2010)
[30] J Halbritter, *Zeit. Phys.* **238(5)**, 466 (1970), http://adsabs.harvard.edu/abs/1970ZPhy..238..466H
[31] H Swan, *SRIMP code an online calculator* (Cornell University), https://www.classe.cornell.edu/~liepe/webpage/researchsrimp.html
[32] J P Turneaure, J Halbritter and Schwettman, *J. Supercond.* **4(5)**, 341 (1991), https://doi.org/10.1007/BF00618215
[33] F Koechlin and B Bonin, *Supercond. Sci. Technol.* **9(6)**, 453 (1996)
[34] L S Sharath Chandra *et al*, *Supercond. Sci. Technol.* **25(3)**, 035010 (2012), https://doi.org/10.1088/0953-2048/25/3/035010
[35] J Bardeen, G Rickayzen and L Tewordt, *Phys. Rev.* **113**, 982 (1959), https://doi.org/10.1103/PhysRev.113.982
[36] S Belomestnykh and H S Padamsee, Cavities for accelerators, *Applied superconductivity: Handbook on devices and applications* edited by P Seidel, 2nd edn (Dover Publication, NY, USA, 2004) Vol. 2, p. 749
[37] H Mittag, *Cryogenics* **13**, 94 (1973)
[38] K Buesser, *School and Workshops on Elementary Particle Physics and Gravity* (Corfu, Greece, 2012) pp. 8–27, arXiv:1306.3126.pdf
[39] W Singer *et al*, *Supercond. Sci. Technol.* **28**, 085014 (2015)
[40] P Dhakal, G Ciovati, P Kneisel and G R Myneni, *IEEE Trans. Appl. Supercond.* **25(3)**, 3500104 (2015), https://doi.org/10.1109/TASC.2014.2359640
[41] G Ciovati, P Dhakal and G R Myneni, *Supercond. Sci. Technol.* **29(6)**, 1 (2016), http://stacks.iop.org/0953-2048/29/i=6/a=064002
[42] H A Leupold and H A Boorset, *Phys. Rev.* **134(5A)**, AB3 (1964), https://doi.org/10.1103/PhysRev.137.AB3
[43] A Grassellino, A Romanenko, D Sergatskov and O Melnychuk, *Supercond. Sci. Technol.* **26**, 102001 (2013), https://doi.org/10.1088/0953-2048/26/10/102001
[44] P Dhakal, G Ciovati, G R Myneni and K E Gray, *Phys. Rev. ST Accel. Beams* **16**, 042001 (2013), https://doi.org/10.1103/PhysRevSTAB.16.042001